

# MRI of pneumonia in immunocompromised patients: comparison with CT

Afra Ekinci  
Tuba Yücel Uçarkuş  
Aylin Okur  
Mehmet Öztürk  
Serap Doğan

## PURPOSE

Pneumonia is an important cause of mortality and morbidity in immunocompromised patients. Computed tomography (CT) is the most sensitive imaging modality for the diagnosis and surveillance of these patients. Since CT exposes the patient to ionizing radiation, we investigated the utility of magnetic resonance imaging (MRI) in the diagnosis and surveillance of immunocompromised patients with pneumonia.

## METHODS

The study included 40 immunocompromised patients with pneumonia documented on CT. The patients were examined by MRI within 48 hours of CT examination. All images were obtained with three different sequences: balanced fast field echo, T1-weighted turbo spin-echo (TSE), and T2-weighted TSE. Lung abnormalities were evaluated using CT and MRI.

## RESULTS

Infection was determined in 36 patients (90%), while the causative organism remained unknown in four patients (10%). In all the patients, the CT findings were consistent with infection, although three patients showed no abnormal findings on MRI. CT was superior to MRI in the detection of the tree-in-bud nodules, centrilobular nodules, and halo sign ( $P < 0.001$ , for all). A significant difference was observed between the MRI sequences and CT in terms of the number of detected nodules ( $P < 0.001$ ). The nodule detection rate of MRI significantly increased in proportion to the size of the nodule ( $P < 0.001$ ). All MRI sequences had almost perfect agreement with CT for the detection of consolidation ( $\kappa=0.950$ ,  $P < 0.001$ ), patchy increased density ( $\kappa=1$ ,  $P < 0.001$ ), pleural effusion ( $\kappa=0.870$ ,  $P < 0.001$ ), pericardial effusion ( $\kappa=1$ ,  $P < 0.001$ ), reverse halo sign, ( $\kappa=1$   $P < 0.001$ ), 10–20 mm, nodules ( $\kappa=0.896$ ,  $P < 0.001$  for CT and B-FFE;  $\kappa=0.948$ ,  $P < 0.001$  for CT and T1- or T2-weighted imaging) 10–20 mm, >20 mm nodules ( $\kappa=0.844$ ,  $P < 0.001$ ).

## CONCLUSION

Although CT is superior to MRI in the diagnosis of pneumonia in immunocompromised patients, MRI is an important imaging modality that can be used, particularly in the follow-up of these patients, thus decreasing to avoid ionizing radiation exposure.

The lungs are often the source of sepsis in immunocompromised patients. If these infections are not treated promptly and effectively in neutropenic patients, mortality can occur. Therefore, early and correct diagnosis is of paramount importance. While certain patterns may point toward a specific organism, the infectious agent cannot always be revealed (1, 2).

Although computed tomography (CT) has the disadvantage of ionizing radiation exposure, it is accepted as the most sensitive test in radiologic evaluation of the lungs. However, because pulmonary infections are often encountered in immunocompromised patients, it may be necessary to repeat the test for diagnosis and during treatment surveillance (3, 4).

Magnetic resonance imaging (MRI), in which there is no radiation exposure, is rarely used for the evaluation of pulmonary parenchyma because of the low proton content of the lungs and possible respiratory and cardiac pulsation artifacts (5). However, MRI has some advantages over CT, such as the provision of high soft-tissue contrast, the ability to better characterize tissue, and the lack of ionizing radiation.

In this study, we investigated the utility of MRI in the diagnosis and surveillance of pulmonary infections in comparison with CT.

From the Department of Radiology (A.E. ✉ [drafrayildirim@hotmail.com](mailto:drafrayildirim@hotmail.com), S.D.), Erciyes University School of Medicine, Kayseri, Turkey; the Department of Radiology (T.Y.U.), Kayseri Training and Research Hospital, Kayseri, Turkey; the Department of Radiology (A.O.), Bozok University School of Medicine, Yozgat, Turkey; Diyarbakir Children's Hospital (M.Ö.), Diyarbakir, Turkey.

Received 5 February 2016; revision requested 26 March 2016; last revision received 5 May 2016; accepted 24 May 2016.

Published online 9 September 2016.  
DOI 10.5152/dir.2016.16055

## Methods

### Patients and clinical assessment

Institutional review board approval was obtained for this prospective study, and written informed consent was obtained from each participant prior to the study.

The study included immunocompromised patients, as determined by positive findings on thoracic CT obtained in the radiology department for suspected pulmonary infection, who were followed up in the hematology, oncology, infectious diseases, nephrology, and bone marrow transplantation clinics. Patients receiving immunosuppressive treatment and/or neutropenic patients (peripheral blood polymorphonuclear leukocyte and band neutrophil value  $<500/\text{mm}^3$ ) were accepted as immunocompromised. Immunocompetent patients and children younger than 18 years of age were excluded from the study. MRI was performed within 48 hours of CT examination. Patients were excluded if they could not undergo MRI due to the severity of illness or claustrophobia ( $n=15$ ) or if the MRI was nondiagnostic, e.g., because of artifacts ( $n=3$ ). The final study cohort consisted of 40 patients: 31 males (77.5%) and nine females (22.5%), with a mean age of  $46.3 \pm 13.7$  years (range, 18–77 years). The study group comprised patients with hematologic malignancy, hematopoietic diseases, solid organ tumor, and autoimmune disease receiving immunosuppressive treatment: 19 patients (47.5%) with acute myeloid leukemia (AML), eight patients (20%) with acute lymphocytic leukemia, four patients (10%) with non-Hodgkin lymphoma, two patients (5%) with chronic lymphocytic leukemia, two patients (5%) with multiple myeloma, one patient (2.5%) with paroxysmal nocturnal hemoglobinuria (PNH); one patient (2.5%) with myelodysplastic syndrome (MDS), one patient (2.5%) with idiopathic thrombocytopenic purpura

(ITP), one patient (2.5%) with systemic lupus erythematosus, one patient (2.5%) with nasopharyngeal carcinoma. Two patients (one with multiple myeloma, the other with ITP) underwent autologous hematopoietic stem cell transplantation (HSCT) and six patients (with AML, PNH, and MDS) underwent allogeneic HSCT. The clinical and laboratory findings were obtained for all patients. The microbiologic and serologic laboratory results and clinical observations were taken as the basis for the identification of the infection agent. Diagnosis of bacterial infection was made by obtaining a culture from the sputum or bronchoalveolar lavage (BAL) or pleural fluid. Cytomegalovirus (CMV) was diagnosed using a positive IgM serology or by the detection of CMV DNA with polymerase chain reaction in blood. Sample (sputum, BAL, pleural fluid) culture, galactomannan, and 1,3-beta-D-glucan tests were used for the diagnosis of fungal infection. The demographic and clinical features of the patients are shown in Table 1.

### Thoracic CT technique

The CT examination was acquired at a multidetector CT scanner (Light Speed 16, GE Medical systems). Unenhanced images were obtained from the level of the hypopharynx to the base of the lungs using the following parameters; 120 kVp, 140 mAs, pitch 1, collimation of 1–2 mm, average scan time of 9 s. Images were formed at slice thicknesses of 10 and 1.25 mm. Evaluation was performed using a mediastinal (level 45, range 440) and lung parenchymal window (level -500, range 2000).

### Thoracic MRI technique

MRI was performed within 48 hours of the CT examination using a 1.5 Tesla scanner (Philips Gyroscan Intera, Philips Medical Systems). For each patient, MRI was performed in the axial and coronal planes using T2-weighted balanced fast field echo (B-FFE), T1-weighted turbo spin-echo (TSE), and T2-weighted TSE sequences. For the T1- and T2-weighted TSE sequences, a sensory body coil was used (slice thickness, 6 mm; gap, 1 mm). The repetition time value was in the range of 1700–2200 for T1-weighted, 3900–4900 for T2-weighted, and 3.1–3.6 for B-FFE sequences. The echo time value was 11 for T1-weighted, 90 for T2-weighted, and 2 for B-FFE sequences. A matrix of  $256 \times 256$ , field of view of 400–455 mm, and flip angle of 60–90 were used. The examination times were 13–19 s, 3.0–3.9 min, and 1.3–1.9

min on coronal B-FFE, T1-, and T2-weighted sequences and 11–17 s, 2.4–3.8 min, and 1.5–2.2 min on axial B-FFE, T1-, and T2-weighted sequences, giving a total of 31 processes with a mean of 8.6–12.4 min. The B-FFE sequences were taken with the patient holding his or her breath, while respiratory triggering technique was used in the other sequences. No contrast material was used.

### Image interpretation

The CT and MRI data were evaluated on a picture archiving and communication system (PACS). Two radiologists (2 and 5 years' experience in thoracic imaging) performed the image evaluation on consensus. Both radiologists were blinded to all the clinical information. CT and MRI data were reviewed separately on different days. The images were interpreted with respect to the nodules, consolidation, ground glass appearance, patchy increased density, cavity, bronchodilation, peribronchial thickening, pericardial fluid and thickening, centrilobular nodules, tree-in-bud nodules, interlobular septal thickening, halo sign, air-crescent sign, and reverse halo sign. The nodule diameters were classified into four groups:  $<5$  mm, 5–10 mm, 10–20 mm, and  $>20$  mm, on the thorax CT and/or MRI images. Bacterial infection was suggested by the presence of consolidation and a ground glass appearance with pleural fluid on CT. Nodules with a halo sign, air-crescent sign, and cavity on CT were assumed to be fungal infection. Centrilobular nodules, peribronchial thickening, interlobular septal thickening, tree-in-bud nodules, and a ground glass appearance were assumed to be viral infection based on the CT findings.

### Statistical analysis

Statistical analyses were performed with a commercially available software package (Statistical Package for Social Sciences, Version 15.0, SPSS Inc.). In the comparison of the qualitative data, the Fisher-Freeman-Halton test was used, and a value of  $P < 0.05$  was accepted as statistically significant. To determine the degree of agreement between the CT and MRI sequences, Cohen's Kappa coefficients were calculated. A Kappa coefficient value of  $<0.00$  was accepted as poor agreement, 0.00–0.20 as slight, 0.21–0.40 as fair, 0.41–0.60 as moderate, 0.61–0.80 as substantial, and 0.81–1.00 as almost perfect agreement (6).

#### Main points

- In this study, we found no significant difference between MRI and CT in the demonstration of most parenchymal and pleural findings in immunocompromised patients with pneumonia.
- Use of MRI instead of CT can prevent repetitive radiation exposure, particularly in surveillance of immunocompromised young patients with pneumonia.
- MRI can be an alternative to CT in diagnosis of pulmonary infection in selected patients.

**Table 1.** Demographic and clinical features of patients

Patient No	Age (years)	Sex	Primary disease	Infectious agent
1	58	M	AML	<i>Aspergillus</i>
2	38	M	NHL	<i>Aspergillus</i>
3	40	M	AML	-
4	66	F	AML	<i>Staphylococcus aureus</i>
5	48	M	ITP, autologous HSCT	<i>Staphylococcus aureus</i>
6	54	M	AML	<i>Aspergillus</i>
7	58	M	NHL	<i>Aspergillus</i>
8	48	M	SLE	<i>Aspergillus</i>
9	66	M	CLL	<i>Aspergillus</i>
10	47	M	MM, autologous HSCT	<i>Aspergillus</i>
11	48	M	AML, allogeneic HSCT	<i>Candida albicans</i>
12	35	F	AML, allogeneic HSCT	CMV
13	36	M	PNH, allogeneic HSCT	<i>Aspergillus</i>
14	64	M	AML	<i>Aspergillus</i>
15	50	M	Nasopharyngeal carcinoma	<i>Staphylococcus aureus</i>
16	27	M	ALL	<i>Aspergillus</i>
17	58	F	ALL	<i>Aspergillus</i>
18	62	M	ALL	<i>Stenotrophomonas maltophilia</i>
19	18	M	ALL	-
20	32	M	ALL	<i>Aspergillus</i>
21	31	M	ALL	-
22	32	M	AML	<i>Acinetobacter baumani</i>
23	34	M	AML	<i>Aspergillus</i>
24	44	F	AML, allogeneic HSCT	CMV
25	53	F	AML	CMV
26	30	M	AML, allogeneic HSCT	<i>Aspergillus</i>
27	35	M	AML	<i>Aspergillus</i>
28	52	M	ALL	<i>Klebsiella oksitoca</i>
29	32	F	AML	<i>Aspergillus</i>
30	54	M	ALL	<i>Acinetobacter baumannii</i>
31	44	M	MDS, allogeneic HSCT	CMV
32	77	F	NHL	CMV
33	54	M	AML	CMV
34	18	M	AML, allogeneic HSCT	CMV
35	69	M	NHL	<i>Aspergillus</i>
36	52	M	MM, autologous HSCT	<i>Escherichia coli</i>
37	42	F	AML	<i>Klebsiella pneumoniae</i>
38	43	M	AML, allogeneic HSCT	-
39	54	M	CLL	<i>Nocardia asteroides</i>
40	50	F	AML	<i>Aspergillus</i>

M, male; F, female; AML, acute myeloid leukemia; NHL, non-Hodgkin lymphoma; ITP, idiopathic thrombocytopenic purpura; HSCT, hematopoietic stem cell transplantation; SLE, systemic lupus erythematosus; CLL, chronic lymphocytic leukemia; MM, multiple myeloma; PNH, paroxysmal nocturnal hemoglobinuria; ALL, acute lymphocytic leukemia; MDS, myelodysplastic syndrome; CMV, cytomegalovirus.

## Results

Of the 40 patients, fungal infection was determined in 19 (47.5%), bacterial infection in 10 (25%), and cytomegalovirus infection in seven (17.5%) patients; in four patients (10%), the pathogenic agent could not be determined. While the findings of infection were seen in CT images of all the cases, MRI was normal in three cases (the rate of positive findings on MRI was 92.5%). Of the three patients in which positive findings were not observed on MRI, one nodule of <5 mm was detected on CT in one patient; four nodules of <5 mm and one nodule of 5–10 mm were detected in another patient; and seven nodules of <5 mm, one nodule of 5–10 mm, centrilobular nodules, a cavity of 7 mm diameter, and tree-in-bud nodules were detected on CT in the third patient (Figs. 1 and 2).

CT was determined to be superior to MRI in showing the tree-in-bud nodules ( $P < 0.001$ ), centrilobular nodules ( $P < 0.001$ ), and halo sign ( $P = 0.001$ ) (Table 2, Fig. 3). No statistically significant difference was determined between CT and MRI in the demonstration of consolidation, a ground glass appearance, patchy increased density, cavity, bronchodilation, peribronchial thickening, interlobular septal thickening, pericardial effusion, pleural thickening, air-crescent sign, and reverse halo sign (Table 2). In three patients, minimal pleural effusion was observed on MRI but not on CT, although this difference was not statistically significant ( $P = 0.902$ ) (Fig. 4). Of the 337 total nodules determined in 40 patients on CT, 170 (51%) could be determined on T2-weighted TSE, 158 (47%) on T1-weighted TSE, and 104 (31%) on B-FFE. On the MRI sequences, most nodules were determined on the T2W-TSE sequences. A statistically significant difference was found between MRI and CT with respect to the number of nodules determined ( $P < 0.001$ ). As the nodule size increased, so did the rate of nodule determination on MRI ( $P < 0.001$ ).

All MRI sequences had slight agreement with CT for the detection of tree-in-bud nodules ( $\kappa=0.178$ ,  $P = 0.048$ ) and centrilobular nodules ( $\kappa=0.113$ ,  $P = 0.122$ ). All MRI sequences had fair agreement with CT for nodules smaller than 5 mm in diameter. The B-FFE sequence had fair agreement with CT for the detection of halo and air-crescent signs. The agreement between the CT and MRI sequences for the detection of lung abnormalities are shown in Table 3. No

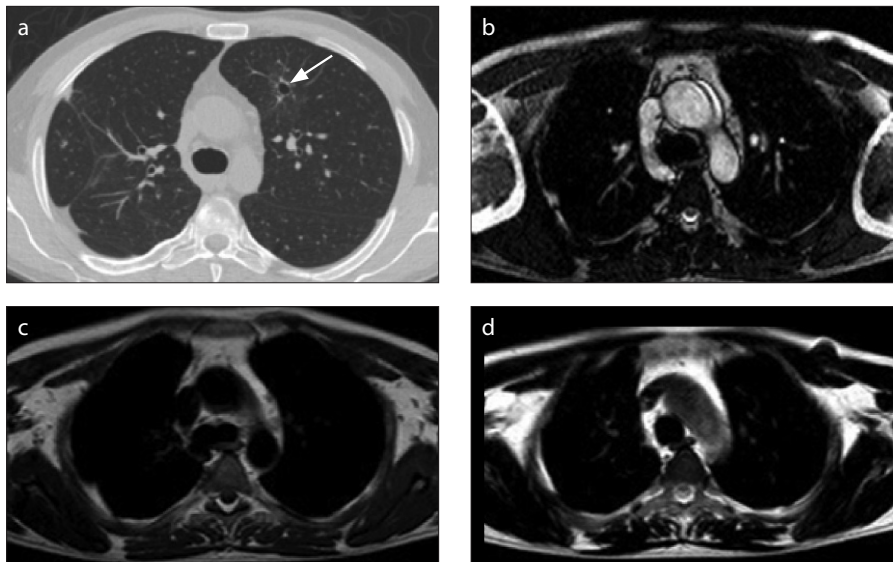


**Figure 1. a–d.** A 31-year-old man with ALL. Infectious agent could not be found. CT image (a) shows 7 mm diameter cavity (arrow). Cavity cannot be seen on B-FFE (b), T1-weighted (c), or T2-weighted (d) images.

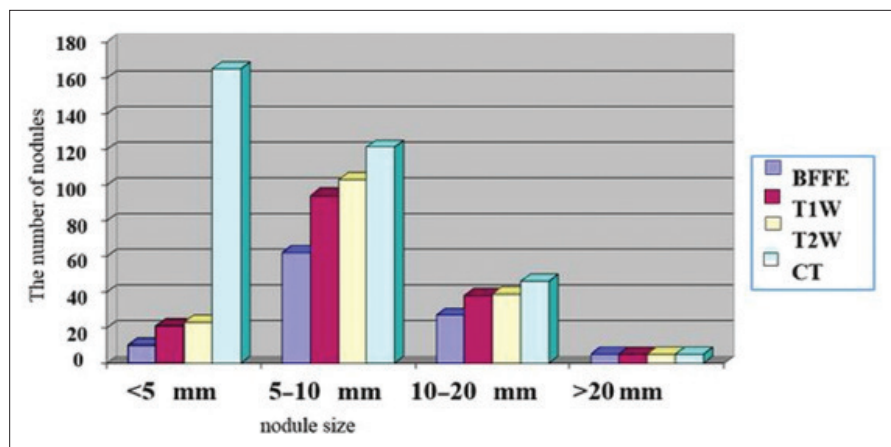


**Figure 2.** The numbers of nodules detected on MRI sequences and CT according to nodule size. BFFE, balanced fast field echo; T1W, T1-weighted; T2W, T2-weighted; CT, computed tomography.

kappa coefficient statistics were computed because the interlobular septal thickening was a constant in all MRI sequences.

## Discussion

This study demonstrated that there was no significant difference between CT and MRI in the assessment of most parenchymal and pleural findings. Compared with other MRI sequences, better results were provided by T2-weighted TSE sequences in the evaluation of parenchymal nodules.

The first, most basic, and freely available radiologic examination method for the lungs is thoracic radiography. The development of CT and then spiral and multi-detector CT, which give much more useful information than pulmonary radiography,

has enabled the rapid examination of a high-quality image of the thorax within the duration of a single breath-hold (5). CT is often used in the imaging of the lungs and provides valuable data for clinical diagnosis, but the penalty of ionizing radiation and its potential mutagenic effect are of concern (7). In particular, in young patients who require frequent follow-up and who may need to undergo multiple CT scans, which can result in a high cumulative dose of radiation (3, 4). It has been reported that a CT examination of approximately 10 mSv is associated with a 1/2000 possibility of fatal cancer development during the lifetime of a patient (8). Therefore, when selecting an examination method, if there are other methods that can provide the same infor-

mation without using ionizing radiation, those should be selected. Thoracic CT doses were approximately 5 mSv in our study.

In the past, MRI was not accepted as an effective method of pulmonary evaluation because of low proton density, susceptibility artifacts due to the air-tissue interfaces, low signal intensity, respiratory and cardiac pulsation artifacts, and weak resolution (9). In addition, the longer duration of MRI application severely restricted its use. Current navigation techniques, which compensate for moving artifacts, and the development of sequences aimed at minimizing the negative effects of respiratory movements by providing the acquisition of rapid images have significantly increased image quality in pulmonary evaluation and relatively shortened the test duration. Thus, MRI evaluation of the pulmonary parenchyma has reached a level comparable to that of CT (10). Among patients who have hematologic malignancies and have undergone chemotherapy, fungal and bacterial infection of the lung is a frequent serious pulmonary complication in those who are immunocompromised. In particular, fungal infection of the lung often has a rapid and fatal course. An early and accurate diagnosis of infection is important to improve patient survival. MRI can be used for the diagnosis of pulmonary infection that has high mortality and needs fast treatment and would be particularly useful in case of delayed sample culture or impossible conditions of tissue sampling for culture such as hypoxemia or thrombocytopenia.

The CT findings of pulmonary infections in immunocompromised patients have been described in the literature (11). In many studies of pulmonary infections in immunocompromised patients performed with various MRI sequences, the findings on CT and MRI have been compared. The most frequently used sequences are T2-weighted half Fourier single-shot turbo spin-echo (HASTE) (12–14), the T2-weighted ultrashort spin-echo (SE) sequence (15), and the T2- and T1-weighted turbo spin-echo (TSE) sequences (16). However, few studies have compared different MRI sequences (16). Previous studies have shown a significant reduction in signal loss and artifact movement in the T2-weighted TSE sequence compared with the T1-weighted SE sequence (17, 18).

In the present study, the rapid-gradient echo sequence B-FFE was used to compensate for the short T2\* duration of the

**Table 2.** Rate of lesion detection for CT and MRI

	B-FFE	T1W	T2W	CT	P
Consolidation	18/40 (45)	18/40 (45)	18/40 (45)	19/40 (47.5)	1.000
Ground glass appearance	7/40 (17.5)	9/40 (22.5)	9/40 (22.5)	14/40 (35)	0.324
Patchy increased density	3/40 (7.5)	3/40 (7.5)	3/40 (7.5)	3/40 (7.5)	1.000
Cavity	4/40 (10)	4/40 (10)	4/40 (10)	6/40 (15)	0.921
Bronchodilation	2/40 (5)	3/40 (7.5)	3/40 (7.5)	4/40 (10)	0.975
Peribronchial thickening	3/40 (7.5)	4/40 (10)	3/40 (7.5)	5/40 (12.5)	0.933
Interlobular septal thickening	0/40 (0)	0/40 (0)	0/40 (0)	1/40 (2.5)	1.000
Pericardial effusion	3/40 (7.5)	3/40 (7.5)	3/40 (7.5)	3/40 (7.5)	1.000
Pleural thickening	2/40 (5)	2/40 (5)	2/40 (5)	3/40 (7.5)	1.000
Air-crescent sign	1/40 (2.5)	3/40 (7.5)	3/40 (7.5)	4/40 (10)	0.690
Reverse halo sign	1/40 (2.5)	1/40 (2.5)	1/40 (2.5)	1/40 (2.5)	1.000
Pleural effusion	17/40 (42.5)	17/40 (42.5)	17/40 (42.5)	14/40 (35)	0.902
Tree-in-bud nodules	2/40 (5)	2/40 (5)	2/40 (5)	14/40 (35)	<0.001
Centrilobular nodules	1/40 (2.5)	1/40 (2.5)	1/40 (2.5)	12/40 (30)	<0.001
Halo sign	7/40 (17.5)	20/40 (50)	23/40 (57.5)	26/40 (65)	0.001

Data are presented as n/N (%).

CT, computed tomography; MRI, magnetic resonance imaging; B-FFE, balanced fast field echo; T1W, T1-weighted imaging; T2W, T2-weighted imaging.

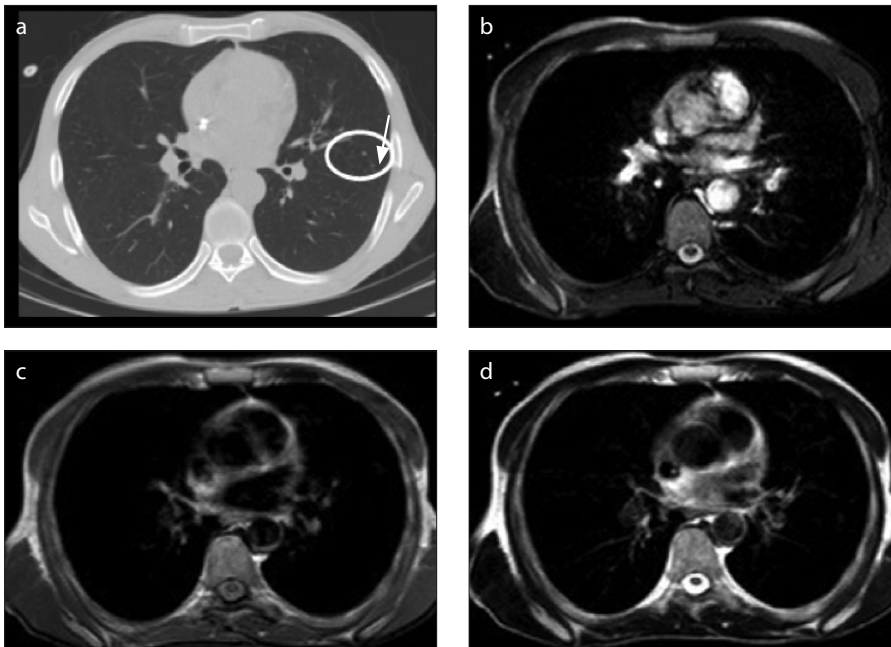


**Figure 3. a–d.** A 31-year-old man with AML and invasive pulmonary aspergillosis. CT image (a) shows centrilobular nodules (arrow). There is no finding on B-FFE (b), T1-weighted (c), or T2-weighted (d) images.

lungs, and T1- and T2-weighted TSE sequences were used as they provide high image contrast and are used in routine MRI examinations. On B-FFE sequences, the goal is to reduce respiratory artifacts to a minimum via the holding of the breath in cooperative patients. Because the test du-

ration is longer for T1- and T2-weighted TSE sequences, the respiratory triggering technique was used. In the current study, we attempted to show the consolidation and ground glass appearance seen on CT by identifying consolidation and lobar and, in some patients, segmental anatomic local-

ization on MRI. In a study by Leutner et al. (15) of 16 immunocompromised patients with CT slices taken at 8 mm, the number and morphology of pulmonary lesions associated with pneumonia shown on CT and MRI (1.5 T, T2-weighted ultrashort SE) were similar in 75% of patients. In the determination of consolidation and a ground glass appearance, both tests gave similar results. In a study by Eibel et al. (13) of 30 neutropenic patients with CT slices taken at 1 mm thickness, a diagnosis of pneumonia could be reached by MRI (1.5 T, T2-weighted HASTE) in 95% of patients. MRI identified all nodules >10 mm and 72% of nodules regardless of size. The halo sign was shown at a rate of 91% by MRI, and a ground glass appearance and parenchymal consolidations were determined at the same rate in both examinations.

Rieger et al. (14) examined 50 neutropenic patients with CT slices taken at 1 mm slice thickness, and a pneumonia diagnosis was made in 91% of patients with MRI (1.5 T, T2-weighted HASTE). In the determination of nodules and the halo sign, in addition to consolidation and a ground glass appearance, both tests were seen to give the same results. However, no information was given about the size of the pulmonary nodules. In a study by Attenberger et al. (18), pulmonary abnormalities were detected with a sensitivity of 82.3%, specificity of 78.6%, and an overall accuracy of 88% in neutropenic patients with AML using 3.0 T MRI. In another study performed with 3.0 T MRI, pulmonary lesions were detected with a high accuracy compared with MDCT in patients with invasive fungal infection (20). In the current study, CT slices were taken at a thickness of 1.25 mm, and evaluations were performed using three separate MRI sequences. For all the MRI sequences, pulmonary abnormality was determined at a rate of 92.5%, and this rate was consistent with many studies in the literature. A ground glass appearance and parenchymal consolidations were determined at the same rate in both examinations, which was also consistent with the literature. In the evaluation of pulmonary nodules, the results taken with T2-weighted TSE were better, and 86% of nodules >10 mm were shown with the T2-weighted TSE sequence. Regardless of size, 51% of nodules could be determined on T2-weighted TSE, 47% on T1-weighted TSE, and 31% on B-FFE.

In the current study, the halo sign could be seen at a rate of 88.5% on T2-weighted TSE,

**Table 3.** Agreement between CT and MRI sequences for the detection of lung abnormalities

	CT and B-FFE	CT and T1W	CT and T2W
Consolidation	$\kappa=0.950, P < 0.001$	$\kappa=0.950, P < 0.001$	$\kappa=0.950, P < 0.001$
Patchy increased density	$\kappa=1, P < 0.001$	$\kappa=1, P < 0.001$	$\kappa=1, P < 0.001$
Ground glass opacity	$\kappa=0.565, P < 0.001$	$\kappa=0.701, P < 0.001$	$\kappa=0.701, P < 0.001$
Cavity	$\kappa=0.773, P < 0.001$	$\kappa=0.773, P < 0.001$	$\kappa=0.773, P < 0.001$
Tree-in-bud nodules	$\kappa=0.178, P = 0.048$	$\kappa=0.178, P = 0.048$	$\kappa=0.178, P = 0.048$
Centrilobular nodules	$\kappa=0.113, P = 0.122$	$\kappa=0.113, P = 0.122$	$\kappa=0.113, P = 0.122$
Bronchodilation	$\kappa=0.643, P < 0.001$	$\kappa=0.844, P < 0.001$	$\kappa=0.844, P < 0.001$
Peribronchial thickening	$\kappa=0.724, P < 0.001$	$\kappa=0.875, P < 0.001$	$\kappa=0.724, P < 0.001$
Pleural effusion	$\kappa=0.870, P < 0.001$	$\kappa=0.870, P < 0.001$	$\kappa=0.870, P < 0.001$
Pleural thickening	$\kappa=0.787, P < 0.001$	$\kappa=0.787, P < 0.001$	$\kappa=0.787, P < 0.001$
Pericardial effusion	$\kappa=1, P < 0.001$	$\kappa=1, P < 0.001$	$\kappa=1, P < 0.001$
Halo sign	$\kappa=0.318, P = 0.006$	$\kappa=0.808, P < 0.001$	$\kappa=0.875, P < 0.001$
Air-crescent sign	$\kappa=0.375, P = 0.002$	$\kappa=0.643, P < 0.001$	$\kappa=0.643, P < 0.001$
Reverse halo sign	$\kappa=1, P < 0.001$	$\kappa=1, P < 0.001$	$\kappa=1, P < 0.001$
Total nodule	$\kappa=0.522, P < 0.001$	$\kappa=0.662, P < 0.001$	$\kappa=0.662, P < 0.001$
Nodule <5 mm	$\kappa=0.226, P = 0.024$	$\kappa=0.261, P = 0.014$	$\kappa=0.297, P = 0.008$
Nodule 5–10 mm	$\kappa=0.744, P < 0.001$	$\kappa=0.787, P < 0.001$	$\kappa=0.787, P < 0.001$
Nodule 10–20 mm	$\kappa=0.896, P < 0.001$	$\kappa=0.948, P < 0.001$	$\kappa=0.948, P < 0.001$
Nodule >20 mm	$\kappa=0.844, P < 0.001$	$\kappa=0.844, P < 0.001$	$\kappa=0.844, P < 0.001$

CT, computed tomography; MRI, magnetic resonance imaging; B-FFE, balanced fast field echo; T1W, T1-weighted imaging; T2W, T2-weighted imaging.

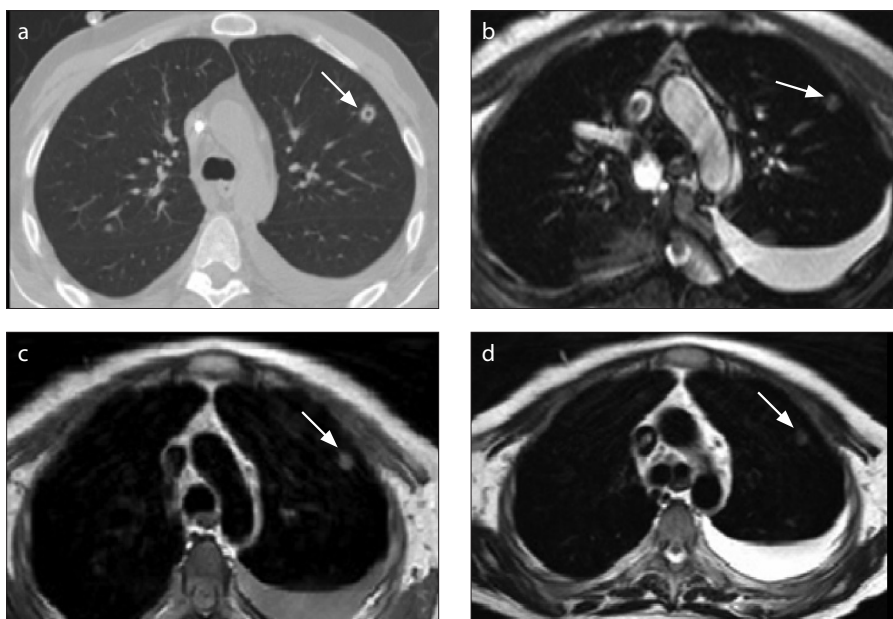


**Figure 4.** a–d. A 38-year-old man with Burkitt lymphoma and invasive pulmonary aspergillosis. CT image (a) shows cavitating nodule (arrow) in the left upper lobe and left pleural effusion. B-FFE (b), T1-weighted (c), and T2-weighted (d) images show a nodule (arrow) and the pleural effusion. The cavity in the nodule is not seen on MRI.

at 76.9% on T1-weighted TSE, and at 26.9% on B-FFE. No study could be found in the literature that compared the two tests with

respect to centrilobular nodules and tree-in-bud nodules. In the current study, 14% of tree-in-bud nodules and 8% of centrilobular

nodules were seen on MRI. The difference between CT and MRI in the demonstration of these findings was statistically significant. In a study by Kersjes et al. (17), the determination of metastatic nodules in 23 patients was compared between CT and MRI (1.5 T, T2-weighted TSE, slice thickness 5 mm). Of all the nodules, 84% could be determined with the T2-weighted TSE sequence. Nodules <5 mm were determined at a rate of 36% by MRI, 5–10 mm at 83%, 10–15 mm at 92%, and >15 mm at 100%. Of the nodules determined on CT in the current study, 51% could be seen on T2-weighted TSE, 47% on T1-weighted TSE, and 31% on B-FFE. On T2-weighted TSE, nodules <5 mm were determined at 14%, 5–10 mm at 85%, 10–20 mm at 85%, and >20 mm at 100%.

Because MRI is a fluid-suppressing examination, there is increased value in the demonstration of changes, such as consolidation and pleural fluid, which are basic pathologic processes in pulmonary infections (21). In the current study, pleural fluid was observed in 14 patients on CT and in 17 patients on MRI sequences. In three patients in which fluid was not observed on CT, minimal fluid was seen on MRI, but this difference was not statistically significant.

This study had certain limitations. Although the number of cases in the study group was good in comparison with the literature, it was not sufficient for the calculation of true positive and negative predictive values. The primary factor limiting the number of cases was patient inability to tolerate MRI on the basis of the severity of their illness. Another limitation is that the MRI sequence was performed without intravenous administration of contrast medium. Therefore, differentiation of active inflammation from fibrosis and detection of smaller lung nodules were not explored.

In conclusion, the results of this study showed no significant difference between MRI and CT in the demonstration of most parenchymal and pleural findings. CT was superior to MRI in the visualization of the tree-in-bud nodules, centrilobular nodules, and the halo sign. In the evaluation of parenchymal nodules, the best results were obtained with T2-weighted TSE, and the worst results were obtained with B-FFE. Therefore, in the evaluation of nodules, the T2-weighted TSE sequence should be selected. The majority of nodules >10 mm can be seen on MRI, but MRI is not sufficient to show nodules <5 mm. Slice thick-

ness, which is thinner for CT than for MRI, is an important factor affecting the ability to determine lesions. In young patients in which continuous imaging is performed for the evaluation of the response to treatment or the progression of disease, MRI may be an alternative modality to CT. MRI can make a diagnosis of pneumonia requiring antimicrobial or expensive systemic antifungal treatment. Therefore, it can reduce costs and provide an accurate treatment decision. The use of MRI instead of CT can prevent repetitive radiation exposure, especially in the surveillance of immunocompromised young patients with pneumonia. More extensive studies are required with patients with different pulmonary pathologies to improve the image quality and standardize the acquisition protocol.

### Conflict of interest disclosure

The authors declared no conflicts of interest.

### References

- Gazzoni FF, Hochhegger B, Severo LC, et al. High-resolution computed tomographic findings of Aspergillus infection in lung transplant patients. *Eur J Radiol* 2014; 83:79–83. [\[CrossRef\]](#)
- Chu H, Li B, Zhao L, et al. Tree-in-bud pattern of chest CT images for diagnosis of Mycobacterium abscesses. *Int J Clin Exp Med* 2015; 8:18705–18712.
- Richenberg J, Harvey C. The utility of CT in imaging chest infections in HIV-negative patients. *Curr Opin Pulm Med* 1999; 5:179–184. [\[CrossRef\]](#)
- Copley SJ. Application of computed tomography in childhood respiratory infections. *Br Med Bull* 2002; 61:263–279. [\[CrossRef\]](#)
- Prokop M. General principles of MDCT. *Eur J Radiol* 2003; 45:4–10. [\[CrossRef\]](#)
- Landis JR, Koch GG. The measurement of observer agreement for categorical data. *Biometrics* 1997; 33:159–174. [\[CrossRef\]](#)
- Lipscomb M. Environmental diseases. In: Kumar V, Cotran R, Robbins S (eds). *Basic pathology*. 5th ed. Philadelphia; W.B.Saunders, 1992: 217–274.
- Committee to Assess Health Risks from Exposure to Low Levels of Ionizing Radiation; Nuclear and Radiation Studies Board, Division on Earth and Life Studies, National Research Council of the National Academies. *Health risks from exposure to low levels of ionizing radiation: BEIR VII Phase 2*. Washington, DC: The National Academies Press; 2006.
- Ohno Y, Koyama H, Yoshikawa T, et al. Pulmonary magnetic resonance imaging for airway diseases. *J Thorac Imaging* 2011; 26:301–316. [\[CrossRef\]](#)
- Bittner RC, Felix R. Magnetic resonance (MR) imaging of the chest: state of the art. *Eur Respir J* 1998; 11:1392–1404. [\[CrossRef\]](#)
- Demirkazik FB, Akin A, Uzun O, Akpınar MG, Ariyürek MO. CT findings in immunocompromised patients with pulmonary infections. *Diagn Interv Radiol* 2008; 14:75–82.
- Hatabu H, Gaa J, Tadamura E, et al. MR imaging of pulmonary parenchyma with a half fourier single-shot turbo spin-echo (H) sequence. *Eur J Radiol* 1999; 29:152–159. [\[CrossRef\]](#)
- Eibel R, Herzog P, Dietrich O, et al. Pulmonary abnormalities in immunocompromised patients: comparative detection with parallel acquisition MR imaging and thin-section helical CT. *Radiology* 2006; 241:880–891. [\[CrossRef\]](#)
- Rieger C, Herzog P, Eibel R, Fiegl M, Ostermann H. Pulmonary MRI—a new approach for the evaluation of febrile neutropenic patients with malignancies. *Support Care Cancer* 2008; 16:599–606. [\[CrossRef\]](#)
- Leutner CC, Gieske J, Lutterbey G, et al. MR imaging of pneumonia in immunocompromised patients comparison with helical CT. *AJR Am J Roentgenol* 2000; 175:391–397. [\[CrossRef\]](#)
- Blum U, Windfuhr M, Buitrago-Tellez C, Sigmund G, Herbst EW, Langer M. Invasive pulmonary aspergillosis. MRI, CT, and plain radiographic findings and their contribution for early diagnosis. *Chest* 1994; 106:1156–1161. [\[CrossRef\]](#)
- Kersjes W, Mayer E, Buchenroth M, Schunk K, Fouda N, Cagil H. Diagnosis of pulmonary metastases with turbo-SE MR imaging. *Eur Radiol* 1997; 7:1190–1194. [\[CrossRef\]](#)
- Lutterbey G, Gieseke J, Sommer T. A new application of MR tomography of the lung using ultra-short turbo spin echo sequences. *Rofo* 1996; 164:388–393. [\[CrossRef\]](#)
- Attenberger UI, Morelli JN, Henzler T, et al. 3 Tesla proton MRI for the diagnosis of pneumonia/lung infiltrates in neutropenic patients with acute myeloid leukemia: initial results in comparison to HRCT. *Eur J Radiol* 2014; 83:61–66. [\[CrossRef\]](#)
- Yan C, Tan X, Wei Q, et al. Lung MRI of invasive fungal infection at 3 Tesla: evaluation of five different pulse sequences and comparison with multidetector computed tomography (MDCT). *Eur Radiol* 2015; 25:550–557. [\[CrossRef\]](#)
- Gaeta M, Minutoli F, Ascenti G, et al. MR white lung sign: incidence and significance in pulmonary consolidations. *J Comput Assist Tomogr* 2001; 25:890–896. [\[CrossRef\]](#)